Published in final edited form as:
Acta Biomater. 2009 May ; 5(4): 1338–1348. doi:10.1016/j.actbio.2008.10.023.

Physico-mechanical properties determination using microscale homotopic measurements: Application to sound and caries-affected primary tooth dentin

Orestes Marangos[a,b], **Anil Misra**[a,b,*], **Paulette Spencer**[b,c], **Brenda Bohaty**[d], and **J. Lawrence Katz**[b,c]

a *Civil, Environmental and Architectural Engineering Department, University of Kansas, 1530 W. 15th Street, Lawrence, KS 66045-7609, USA*

b *Bioengineering Research Center (BERC), University of Kansas, 1530 W. 15th Street, Lawrence, KS 66045-7609, USA*

c *Mechanical Engineering Department, University of Kansas, 1530 W. 15th Street, Lawrence, KS 66045-7609, USA*

d *Department of Pediatric Dentistry, University of Missouri-Kansas City, 650 E. 25th Street, Kansas City, MO 64108, USA*

Abstract

Microscale elastic moduli, composition and density have rarely been determined at the same location for biological materials. In this paper, we have performed homotopic measurements to determine the physico-mechanical properties of a second primary molar specimen exhibiting sound and caries-affected regions. A microscale acoustic impedance map of a section through this sample was acquired using scanning acoustic microscopy (SAM). Scanning electron microscopy was then used to obtain mineral mass fraction of the same section using backscattered images. Careful calibration of each method was performed to reduce system effects and obtain accurate data. Resorption, demineralization and hypermineralization mechanisms were considered in order to derive relationships between measured mineral mass fraction and material mass density. As a result, microscale mass density was determined at the same lateral resolution and location as the SAM data. The mass density and the acoustic impedance were combined to find the microscale elastic modulus and study the relationship between microscale composition and mechanical properties.

Keywords

Dentin; Micromechanics; Elastic modulus; Density; Acoustic microscopy

1. Introduction

Properties of calcified tissues, such as bone and dentin, have been a subject of intense research for the past several decades [1]. With the advances in experimental methods, measurement of mechanical and compositional properties has been made possible at increasingly high spatial resolutions. In an effort to understand the relationship between these properties, recently, researchers have used complementary high-resolution experimental methods. However, when

*Corresponding author. Address: Civil, Environmental and Architectural Engineering Department, University of Kansas, 1530 W. 15th Street, Lawrence, KS 66045-7609, USA. Tel.: +1 785 864 1750; fax: +1 785 864 5631. *E-mail address:* amisra@ku.edu (A. Misra).

complementary methods are applied on highly heterogeneous materials, such as calcified tissues, it is especially important that the measurements are performed at the same location. In this paper, we introduce the term “homo-topic” (Greek *homos* = identical and *topos* = place) to describe the measurement of properties performed at the same location of the same sample.

Relatively few attempts have been made to perform homotopic measurements of the microscale elastic moduli, composition and density of calcified tissues. Most of these investigations have used destructive indentation techniques for the micromechanical property determination. In the past decade, some investigators have combined ultra-microindentation or nanoindentation with backscattered scanning electron microscopy (BSEM) to study the relationship between mechanical properties and mineral content for a variety of calcified tissues [2-5]. Nanoindentation has also been used in combination with atomic force microscopy, Fourier-transform infrared microspectroscopy, small angle X-ray scattering and BSEM to relate hardness and elastic modulus to a variety of structural and compositional properties of dentin [6,7]. More recently, nanoindentation has been used with time-of-flight secondary ion mass spectroscopy to image the same regions of in vitro carious lesions in human dental enamel [8].

Non-destructive methods, as an alternative to nanoindentation, have rarely been used for homotopic measurements. The advantage of non-destructive methods is that the sample is preserved in its near natural state for analysis with other complementary techniques. Among the earliest efforts to use non-destructive methods is the work by Katz and Meunier [9], in which the same regions of human and canine osteons were imaged using BSEM and scanning acoustic microscopy (SAM). The contrast in the SAM images was explained upon the basis of mineral density variations observed in the BSEM images. Turner et al. [10] measured elastic moduli using SAM and compared them to nanoindentation measurements obtained at similar locations on adjacent sections. SAM has also been used in conjunction with synchrotron radiation microcomputed tomography [11,12] and in combination with Raman microspectroscopy and nanoindentation [13] to obtain site-matched mechanical and compositional properties.

We have used SAM and scanning electron microscopy (SEM) with backscatter electron detection to characterize a second primary molar specimen exhibiting sound and caries-affected regions. Caries-affected dentin is of clinical significance because composite restorations require the dentist to bond material to this substrate. SAM was used to obtain the microscale acoustic impedance at various locations on the sample, ranging from sound dentin to caries-affected dentin. A BSEM image of the same sample was then acquired and analyzed to determine the mineral mass fraction. Relationships between measured mineral mass fraction and material mass density were derived for sound, carious and caries-affected dentin. These relationships were then used to determine the microscale mass density at the same lateral resolution and location as the SAM data. The data from SAM and SEM were combined to obtain the microscale homotopic physico-mechanical properties. As a result, we can study the relationship between the microscale composition and elastic moduli of sound to caries-affected primary tooth dentin.

2. Background – dentin microstructure and properties

Dentin is the hydrated composite structure that constitutes the body of each tooth, providing both a protective covering for the pulp and serving as a support for the overlying enamel. Dentin is composed of approximately 45–50% inorganic material, 30–35% organic material and 20% fluid by volume. Dentin mineral is a carbonate-rich, calcium-deficient apatite [14]. The organic component is predominantly type I collagen, with a minor contribution from other proteins [15-17]. The apatite mineralites are of very small size and are deposited almost exclusively

within the collagen fibril (see e.g. Arsenault [18]). The interactions between collagen and nanocrystalline mineralite give rise to the stiffness of the dentin structure. The consequent dentin elasticity is an important feature that determines the mechanical behavior of the tooth structure.

The structural characteristics of sound dentin are well known at the microscale (100 μm). Dentin is described as a system of dentinal tubules surrounded by a collar of highly mineralized peritubular dentin [19]. The tubules traverse the structure from the pulp cavity to the region just below the dentin–enamel junction (DEJ) or the dentin–cementum junction. The tubules, which are described as narrow tunnels a few microns or less in diameter, represent the tracks taken by the odontoblastic cells from the pulp chamber to the respective junctions. Tubule density, size and orientation vary from location to location. The density and size are lowest close to the DEJ and highest at the pre-dentin surface at the junction to the pulp chamber. Thus, the porosity of dentin varies from zero to 0.25 from the DEJ to the pulp [20-22]. The rate of change in porosity with depth depends on the tooth type. In primary tooth dentin, the dentinal tubule density and size is, in general, larger than in permanent dentin [21].

The composition of the peritubular dentin is carbonated apatite with very small amounts of organic matrix whereas intertubular dentin, i.e. the dentin separating the tubules, is type I collagen matrix reinforced with apatite. Based upon electron microscopic studies, peritubular dentin in primary teeth has been found to be 2–5 times thicker than that of permanent teeth [23]. The composition of intertubular dentin is primarily mineralized collagen fibrils; the fibrils are described as a composite of a collagen framework and thin plate-shaped carbonated apatite crystals whose *c*-axes are aligned with the collagen fibril axis [24]. In sound dentin, the majority of the mineralized collagen fibrils are perpendicular to the tubules [25]. Water in dentin may be classified as either free or bound. Water is present within the dentinal tubules as pulpal fluid and within the interstitial spaces between collagen fibrils. Based upon experimental chemical microanalyses, bound water is likely present as hydroxyl groups bound to the mineral component [26-28].

Beginning in the 1960s, macroscale elastic moduli of dentin have been measured by a variety of methods as reviewed by Kinney et al. [29]. Using nanoindentation methods, Kinney et al. [30], have measured the elastic modulus of peritubular dentin and intertubular dentin. At somewhat larger, unspecified scales, Katz et al. [31] measured similar values of dentin elastic modulus using SAM. At even higher scales, Lees and Rollins [32] used longitudinal and shear wave velocity measurements, Kinney et al. [33] used resonant ultrasound spectroscopy to determine elastic moduli of millimeter scale samples and John [34] used longitudinal velocity measurements on approximately millimeter thick slices to find location-dependent elastic moduli. Primary tooth dentin mechanical properties have been studied at the nanoscale using nanoindentation [35-37]. Mechanical properties of primary tooth dentin have also been studied at somewhat higher, unspecified scales [38,39]. Mass density measurements were completed more than a century ago. Mass densities of permanent and deciduous dentin were determined by direct measurement of mass and volume of moist dentin slabs [40] and by considering dry powdered fractions of teeth [41,42]. More recently, mineral densities of dentin have been measured using X-ray tomographic microscopy [43] and BSEM [2].

3. Materials and methods

3.1. Primary tooth dentin sample preparation and storage

A primary second molar was collected following normal exfoliation under an approved institutional review board (IRB) protocol at the University of Missouri-Kansas City and stored in phosphate-buffered saline solution containing 0.002% sodium azide to reduce bacterial activity. The tooth is part of an IRB approved clinical study focused upon restoration of primary

teeth with composite resins. The particular tooth used in this study had a restoration placed 18 months before natural exfoliation. The tooth was obtained from the patient within 2 weeks of exfoliation and was stored in phosphate-buffered saline solution with 0.002% sodium azide and refrigerated at 4 °C until sectioning was completed. The recovered sample was sectioned in half buccal-lingually with a diamond saw and then in half in a mesial–distal direction along the long axis of the tooth to yield two complementary halves, each containing the in vivo restoration. The restoration was removed during sectioning. Each sample was photographed after collection with a Nikon SMZ 800[10] (Nikon Instruments Inc., Melville, NY) stereomicroscope using various magnifications. The samples were then refrigerated and stored as before until final analysis. Fig. 1 gives an optical image of the section that was examined in this paper.

3.2. Scanning acoustic microscopy

Over the past two decades, SAM has gained wide recognition as a non-destructive method that can be used to characterize microscale mechanical properties of materials [44]. Numerous researchers have used SAM in pulse-echo mode to directly measure material reflection coefficient and, consequently, acoustic impedance [31,45-48]. A commercially available scanning acoustic microscope (WINSAM 100, Kramer Scientific Instruments GmbH, Herborn, Germany) with a 30 MHz central frequency focused transducer (KSI PT30-002) was used in this study to acquire data in pulse-echo mode. The transducer specifications were as follows: nominal lateral resolution ~100 μm, half aperture angle = 13.4°, focal length = 12.7 mm and −6 dB amplitude bandwidth frequencies of 21.6 and 38 MHz. For soft materials, such as caries-affected dentin, the reflected signal amplitude is weak and high amplification settings have to be used to obtain measurable signals. This received signal is influenced by the saturation effects of system electronics at high amplifications. The accuracy of the calculated micromechanical properties is greatly compromised if the saturation effects are not properly considered. Therefore, calibration curves were developed based upon a methodology that can distinguish the effect of system electronics from the material response [49]. In addition, the surface roughness can be a significant source of scattering, and can therefore affect the interpretation of the acoustic measurements. In the theoretical models used to analyze the SAM data, the surface roughness was assumed to be small compared to the measurement scales. Although, in principle, it is possible to model surface topography in theoretical methods used for deriving properties from SAM, the resultant methods are immensely complicated. Therefore, all the calibration materials were surface polished until no significant change in the reflected signal was observed.

The following calibration materials were used in order to provide a wide range of reflection coefficients and acoustic impedances: tungsten, copper, brass, aluminum, vitreous carbon, silica glass, polyvinyl chloride, polyethylene terephthalate glycol, polycarbonate, polypropylene, high-density polyethylene, low-density polyethylene (LDPE) and polymethylpentene (TPX®). For this set of materials, the acoustic impedance was determined by independently measuring longitudinal wave velocity and material mass density. The longitudinal speed of sound, c, in each of the materials was measured by the time-of-flight method using a 5 MHz contact transducer. The longitudinal speed is related to the constrained elastic modulus, C_{11}, and the density as: $c = (C_{11}/\rho)^{1/2}$. Material density, ρ, was measured by applying Archimedes' principle. The value of the theoretical reflection coefficient (R^{th}) of each material was then determined as follows:

$$R_B^{th} = \frac{Z_B - Z_A}{Z_B + Z_A} \quad (1)$$

where Z_A is the acoustic impedance of coupling fluid ($=\rho_A c_A$) and Z_B is the acoustic impedance of the specimen ($=\rho_B c_B$). Distilled water was used as a coupling fluid in our measurements. The acoustic impedance of distilled water was Z_A = 1.49 MRayl at 24 °C, which corresponded to the average temperature of the water tank.

The above set of materials was then imaged with SAM to obtain time-domain A-scan signals. Care was taken to focus the ultrasonic beam on the sample surface. Subsequently, 32 A-scan signals were acquired and averaged to increase the signal-to-noise ratio. The measured reflected signal was then Fourier transformed. Since the lens aperture angle of the transducer used in our SAM measurement is small, a paraxial approximation could be made and the ultrasonic field near the focal plane could be considered as a plane wave, with the main contribution to the amplitude coming from the ray parallel to the transducer axis. In this case, Eq. (1), which is derived for normal incidence, is also applicable for obtaining the reflection coefficients using SAM measurements. Thus, the SAM-measured Fourier amplitude can be related directly to the independently measured reflection coefficients. Therefore, frequency-dependent correlations were obtained to relate the SAM-measured Fourier amplitudes to the reflection coefficients over the transducer −6 dB frequency bandwidth. Fig. 2 shows the obtained calibration curve at 0 dB amplification setting at the frequency of 21.6 MHz, which is the minimum frequency at the −6 dB Fourier amplitude. The 0 dB amplification setting was used for our measurements in this paper as we were able obtain a measurable signal from all regions of our dentin sample. The SAM-measured Fourier amplitudes are also plotted against the independently measured reflection coefficient as shown by the symbols in Fig. 2. The calibration curve can be used to obtain the reflection coefficient of an unknown material using the following best-fit relationship:

$$V=\left(a_1(\omega)\frac{R(R-1)}{(R+1)}+a_0(\omega)R\right)\frac{V_w^m}{R_w} \tag{2}$$

where V is the measured Fourier amplitude of the unknown substrate, V_w^m is the measured Fourier amplitude of the tungsten target, R is the reflection coefficient of the unknown substrate, R_W is the reflection coefficient of the tungsten target, and $a_1(\omega)$ and $a_0(\omega)$ are frequency-dependent fitting constants, which take the values 0.1 and 0.45 at the frequency of 21.6 MHz. An error analysis was performed using Eq. (2), to obtain the relationship between the errors in reflection coefficients in terms of the measured error in Fourier amplitude (defined as the standard deviation of the Fourier amplitudes at a given frequency) [50]. The error in Fourier amplitude was found to be constant for all the materials and can be attributed to random noise. Conveniently, this error can be represented as a signal-to-noise ratio. Higher reflection coefficient materials are therefore expected to have a high signal-to-noise ratio. The signal-to-noise ratio was measured to vary from 34 to 44 dB for low to high reflectance materials, respectively. The corresponding error in the mean reflection coefficient was found to vary from ~0.90% for low to ~0.25% for high reflectance materials. The above analysis was validated by comparing the predicted reflection coefficients of LDPE and TPX® with those obtained through independent measurements.

For the sample shown in Fig. 1, a C-scan was performed in order to correctly locate the regions of interest. Subsequently, 32 A-scan signals were captured at 300 locations at an amplification setting of 0 dB. At each location, care was taken to verify that the dentin substrate was placed at the focus of the ultrasonic beam and that the transducer axis was normal to the substrate. The locations were selected to be 120 μm apart such that the interrogated substrate area was slightly larger than the nominal lateral resolution of the transducer (~100 μm) and corresponded approximately to the spot-size of the focused acoustic beam. This way, there was minimal overlap in the properties of adjacent locations. The acquired signals were gated and averaged

in order to increase the signal-to-noise ratio. Same gate size was used for all the calculations in this paper. Fast Fourier transform was used to obtain the frequency spectrum of the averaged signal for the frequency domain analysis. The Fourier amplitudes were then converted to reflection coefficients using Eq. (2), and the correlation is shown in Fig. 2.

3.3. Backscattered scanning electron microscopy

BSEM has been widely used for the microscale determination of mineral content of hard tissues [6,51,52]. BSEM images of the same sample used for the SAM studies were acquired using a field-emission environmental SEM (Philips XL30 ESEM-FEG 515, Philips Electron Optics Inc., Hillsboro, OR). The sample was dried with ascending concentrations of alcohol, mounted on aluminum stubs and sputter-coated with carbon. The sample was evaluated by SEM using a variety of magnifications. The intent of the SEM study was to obtain the relative mineral composition of the tooth substrate. To this end, a correlation between the grayscale values and the weight per cent of calcium was created by imaging graphite and hydroxyapatite standards. The graphite standard was assumed not to contain any calcium and the synthetic hydroxyapatite standard was obtained as described in Wieliczka et al. [53]. Care was taken to keep the same settings for all of the measurements, and to ensure that the tooth surface was horizontal to avoid artifacts. The backscattered image grayscale value for graphite was found to be 11 ± 5, while that for the hydroxyapatite standard was 230 ± 5. Assuming a linear variation of grayscale values with the weight% of Ca, we developed a correlation as shown in Fig. 3. At each pixel the mineral mass fraction, m_I, was found in terms of the grayscale value, G, as follows:

$$m_I = \frac{(aG - b)}{39.86} \tag{3}$$

where $a = 0.182$ and $b = 2.00$. The linear correlation was verified by plotting the weight% Ca obtained from energy-dispersive X-ray analysis at five different locations on the tooth substrate.

The BSEM image was obtained at ×50 magnification such that a resolution of 1.7 × 1.7 μm was achieved. The regions of interest were carefully delineated from the BSEM image using the positional information from the SAM image. To ensure lateral resolution compatibility between BSEM and SAM measurements, the regions of interest in the BSEM image were divided into square pixels of 120 × 120 μm (corresponding to SAM pixel size) and the grayscale values were averaged within each pixel. The averages were computed using the values within the upper and lower grayscale thresholds of 230 and 11, respectively, which correspond to the average grayscale value of the hydroxyapatite and graphite standards. The average grayscale value was used to calculate the mineral mass fraction, m_I, for each pixel of regions of interest.

3.4. Compositional relationships based upon BSEM measurements

At the microscale, dentin can be idealized as a two-phase (solid and fluid) or three-component (water, inorganic and organic) composite, as depicted in the phase diagram shown in Fig. 4, which also shows the relevant mass and volume balance relationships. The microscale mass density of dentin may be computed by considering the relative proportions of its major components in terms of mass and volume fractions. Mass fractions for sound permanent dentin are widely quoted to be on average as follows: organic mass fraction, $m_o = 0.2$, mineral mass fraction, $m_I = 0.7$, and water mass fraction, $m_w = 0.1$ [54]. The water mass fraction may be further subdivided into bound water fraction, m_{bw} and free water fraction, m_{vw}. Sound primary tooth dentin is reported to have a lower mineral content [27,55] such that the mass fractions are: $m_o = 0.25$, $m_I = 0.65$ and $m_w = 0.1$. These values are included in Table 1 for reference.

For evaluation of the volume fractions, we define the following densities for the different components: water density, denoted by ρ_w, mineral density, denoted by ρ_I and organic component density, denoted by ρ_o. A wide variation is reported for apatitic mineral density, which ranges from 2.8 to 3.35 g cm^{-3} [26,56]. The density of collagen is also reported to vary from 1.33 to 1.41 g cm^{-3}, based upon measurements performed using kangaroo tail tendon, and adult and embryonic bull hide at various water contents [57]. Similar values, ranging from 1.35 to 1.45 g cm^{-3}, have been reported based upon specific volume measurements of rat tail collagen in different solvents [58]. For the calculations performed in this paper, we have assumed a value of 3.00 g cm^{-3} for the mineral component and 1.40 g cm^{-3} for the organic component. Thus, for sound permanent dentin, the average density is found to be 2.10 g cm^{-3} which is consistent with that reported in the literature [54]. Similarly, for sound primary tooth dentin the density is found to be 2.02 g cm^{-3}. As a result, the volume fractions for sound primary tooth dentin are obtained to be: organic volume fraction, $\phi_o = 0.36$, mineral volume fraction, $\phi_I = 0.44$ and water volume fraction, $\phi_w = 0.20$. Furthermore, the bound or combined water mass fraction, m_{bw}, has been shown from ignition loss studies to be ~0.02 [26-28], which corresponds to a bound water volume fraction, ϕ_{bw}, of 0.04. The free water mass fraction, m_{vw}, is then estimated to be 0.08, resulting in a tubule volume fraction or porosity, ϕ_{vw}, of 0.16. This porosity is within the widely quoted dentin porosity range of zero in the vicinity of the DEJ to 0.25 close to the pulp chamber [59,60]. These values of the component mass densities and the mass and volume fractions are summarized in Table 1 for reference. Since the dentin locations we sampled are close to the pulp chamber, we assume an average porosity, ϕ_{vw}^{ref}, of 0.20 for our subsequent calculations. Therefore, for these locations the following nominal values will be used: $m_I^{ref}=0.624$, $\phi_{ow}^{ref}=0.039$, $\phi_o^{ref}=0.343$ and $\rho^{ref}=1.98$ g,cm^{-3}.

We note that the sample considered in this paper was collected upon normal exfoliation and exhibited carious and caries-affected regions. Therefore, it is expected that the dentin substrate would have undergone a loss in mineral content due to natural resorption. In addition, the locations within the carious regions can be expected to have suffered additional loss of mineral, while those within the caries-affected regions could have experienced increased mineral deposition. In all these cases, the nominal mineral volume $\left(V_I^{ref}\right)$ will be altered by a change in the water volume (ΔV_w), that is

$$V_I^{ref}=V_I+\Delta V_w \tag{4}$$

where V_I is the altered mineral volume. As a result of this change in mineral content, the mass and volume fractions as well as the density of the dentin will be different from the nominal values. For further derivation, we note that the volume fraction of the jth component, ϕ_j, is related to its mass fractions, m_j, through the overall density, ρ and component density, ρ_j, as:

$$\phi_j=\frac{\rho}{\rho_j}m_j \tag{5}$$

Thus, Eq. (4) can be rewritten as:

$$\frac{\rho^{ref}}{\rho_I}m_I^{ref}=\frac{\rho}{\rho_I}m_I+\Delta\phi_w \tag{6}$$

Furthermore, the overall density can be obtained by considering the component masses and volumes as follows:

$$\rho=\frac{M}{V}=\rho_{\mathrm{o}}\phi_{\mathrm{o}}^{\mathrm{ref}}+\rho_{\mathrm{I}}\phi_{\mathrm{I}}+\rho_{\mathrm{w}}\left(\phi_{\mathrm{bw}}^{\mathrm{ref}}+\phi_{\mathrm{vw}}^{\mathrm{ref}}\right)+\rho_{\mathrm{w}}\Delta\phi_{\mathrm{w}} \tag{7}$$

Using Eqs. (5)-(7), we find the following expressions for the density, ρ, and the change in water mass fractions, Δm_{w}, in terms of the nominal values and the measured mineral fraction, m_{I}:

$$\rho=\frac{\rho^{\mathrm{ref}}m_{\mathrm{I}}^{\mathrm{ref}}+\left(\frac{\rho_{\mathrm{I}}}{\rho_{\mathrm{w}}}\right)\left(\rho_{\mathrm{w}}\phi_{\mathrm{vw}}^{\mathrm{ref}}+\rho_{\mathrm{w}}\phi_{\mathrm{bw}}^{\mathrm{ref}}+\rho_{\mathrm{o}}\phi_{\mathrm{o}}^{\mathrm{ref}}\right)}{m_{\mathrm{I}}+\frac{\rho_{\mathrm{I}}}{\rho_{\mathrm{w}}}\left(1-m_{\mathrm{I}}\right)} \tag{8}$$

and

$$\Delta m_{\mathrm{w}}=\frac{\rho^{\mathrm{ref}}m_{\mathrm{I}}^{\mathrm{ref}}\left(1-m_{\mathrm{I}}\right)-m_{\mathrm{I}}\left(\rho_{\mathrm{w}}\phi_{\mathrm{vw}}^{\mathrm{ref}}+\rho_{\mathrm{w}}\phi_{\mathrm{bw}}^{\mathrm{ref}}+\rho_{\mathrm{o}}\phi_{\mathrm{o}}^{\mathrm{ref}}\right)}{\rho^{\mathrm{ref}}m_{\mathrm{I}}^{\mathrm{ref}}+\left(\frac{\rho_{\mathrm{I}}}{\rho_{\mathrm{w}}}\right)\left(\rho_{\mathrm{w}}\phi_{\mathrm{vw}}^{\mathrm{ref}}+\rho_{\mathrm{w}}\phi_{\mathrm{bw}}^{\mathrm{ref}}+\rho_{\mathrm{o}}\phi_{\mathrm{o}}^{\mathrm{ref}}\right)} \tag{9}$$

where m_{I} is obtained from BSEM measurements using Eq. (3) and the change in water mass fractions, Δm_{w}, is defined as:

$$\Delta m_{\mathrm{w}}=\frac{\rho_{\mathrm{w}}}{\rho}\Delta\phi_{\mathrm{w}} \tag{10}$$

4. Results and discussion

4.1. Characterization of primary tooth dentin using SAM

Fig. 5a–c shows the maps of the reflection coefficients of all the 300 locations superimposed upon the optical image. The frequency (normalized count) distribution of the reflection coefficients for each map is shown in Fig. 5d–f, respectively. The reflection coefficient maps were plotted such that the pixel size (=120 μm) is the same as the spacing between measurement locations. As seen from Fig. 5a and d, the reflection coefficient over the sampled locations has a wide variation. This variability is, however, region specific. In Fig. 5d we have also indicated the range of reflection coefficients obtained from the locations within the sound dentin, as well as from locations within enamel. To further analyze their variability, we focus upon the reflection coefficients from the three different regions of the dentin that can be differentiated on the basis of the optical image. Region 1 consists of locations in the tooth interior with a homogeneous milky white coloration and is considered to be sound dentin. The reflection coefficients within region 1 are plotted separately in Fig. 5b. Note that locations that lie within the tooth boundary have been plotted to display the data that are free from edge effects. Regions 2 and 3 consist of locations within the discolored portion of dentin and are considered to be the carious and the caries-affected region, respectively. However, locations within these regions are intermingled with each other and cannot be easily demarcated. The reflection coefficients within regions 2 and 3 are plotted in Fig. 5c. We observe that the reflection coefficients in the sound dentin (region 1) range from 0.35 to 0.56, with a mean (±standard deviation) of 0.49 ± 0.05. The frequency distribution of the reflection coefficients in this region is narrow, as observed from Fig. 5e, indicating that the micromechanical properties of sound dentin are fairly homogeneous. The reflection coefficients in carious and caries-affected dentin (regions 2 and 3) ranged from 0.09 to 0.66, with a mean of 0.51 ± 0.15. The carious locations are expected to have undergone demineralization and, therefore, should have a lower reflection coefficient than sound dentin. The caries-affected region, in contrast, is known to be complex

and has been subdivided into a series of zones [61]. The so-called “transparent zone”, which has been described as hypermineralized, and is often a harder zone, occupies the largest proportion of the caries-affected dentin [62,63]. In contrast to sound dentin, the tubules within the caries-affected dentin are frequently occluded by acid-resistant mineral deposits [61, 64-66]. The increased mineral content at these locations will result in reflection coefficients that are higher than the sound dentin. The frequency distribution given in Fig. 5f confirms the presence of two distinct regions, one with reflection coefficients significantly lower (<0.39) than the average sound dentin value of 0.49 ± 0.05 and the other with reflection coefficients significantly higher (>0.59).

4.2. Characterization of primary tooth dentin density

Fig. 6 shows the BSEM image with the regions of interest delineated. Region 1 in Fig. 6 corresponds to a subset of the sound dentin region of Fig. 5b. Regions 2 and 3 of Fig. 6 correspond exactly to the caries and caries-affected regions 2 and 3 of Fig. 5c. The mineral mass fraction of the sound dentin portion of the sample (region 1) was found to range from 0.50 to 0.58, with a mean of 0.54 ± 0.02. This low value is expected, as this sample was likely undergoing resorption prior to exfoliation. The mineral mass fractions in carious and caries-affected dentin (regions 2 and 3) ranged from 0.09 to 0.66, with a mean of 0.54 ± 0.14. These values parallel the findings for the reflection coefficient discussed in Section 3.1. Locations with lower values correspond to carious dentin that has undergone demineralization, while those with higher values lie within the caries-affected region, which is likely hypermineralized. Since the three regions undergo alteration in mineral mass fractions through different mechanisms, we performed separate analyses for the density calculations for these regions. In the subsequent discussion, we use the superscripts “sr” for sound resorbed dentin and “c” for carious and caries-affected dentin. For region 1, the sound dentin density and the mass and volume fractions have to be corrected to account for resorption. In this case, Eqs. (8) and (9) can be used to find the density of the resorbed dentin, ρ^{sr}, as well as the water mass fraction $m_{\mathrm{vw}}^{\mathrm{sr}}\left(=\Delta m_{\mathrm{w}}^{\mathrm{sr}}+m_{\mathrm{vw}}^{\mathrm{ref}}\right)$, in terms of the nominal values and the measured mineral mass fraction.

In the carious locations (region 2), the calculations have to account for demineralization, while in the caries-affected locations (region 3) these calculations must account for mineral deposition in the tubules. As carious locations within dentin suffer further demineralization, additional water likely occupies the dissolved mineral volume. In caries-affected locations the mineral mass fraction is higher than that of the sound resorbed dentin. In these locations we assume that mineral deposition occurs within the tubules by displacing the tubule water. According to the data in the literature, carious dentin has been observed to have very little volume change [20]. Therefore, we assume that the volume is conserved in the carious and the caries-affected portions of the dentin. Hence, we can utilize Eqs. (8) and (9) to calculate the densities, ρ^{c}, and water mass fractions, $m_{\mathrm{vw}}^{\mathrm{c}}$, of carious and caries-affected dentin in terms of the averaged resorbed dentin density, $\bar{\rho}^{\mathrm{sr}}$, mineral mass fraction, $\bar{m}_{1}^{\mathrm{sr}}$, and water volume fraction, $\bar{\phi}_{\mathrm{vw}}^{\mathrm{sr}}$:

$$\rho^{\mathrm{c}}=\frac{\bar{\rho}^{\mathrm{sr}}\bar{m}_{1}^{\mathrm{sr}}+\left(\frac{\rho_{1}}{\rho_{\mathrm{w}}}\right)\left(\rho_{\mathrm{w}}\bar{\phi}_{\mathrm{vw}}^{\mathrm{sr}}+\rho_{\mathrm{w}}\phi_{\mathrm{bw}}^{\mathrm{ref}}+\rho_{\mathrm{o}}\phi_{\mathrm{o}}^{\mathrm{ref}}\right)}{m_{1}+\frac{\rho_{1}}{\rho_{\mathrm{w}}}\left(1-m_{1}\right)} \tag{11}$$

and

$$m_{vw}^{c}=\frac{\bar{\rho}^{sr}\,\bar{m}_{1}^{sr}\,(1-m_{1})-m_{1}\left(\rho_{w}\bar{\phi}_{vw}^{sr}+\rho_{w}\phi_{bw}^{ref}+\rho_{o}\phi_{o}^{ref}\right)}{\bar{\rho}^{sr}\,\bar{m}_{1}^{sr}+\left(\frac{\rho_{1}}{\rho_{w}}\right)\left(\rho_{w}\bar{\phi}_{vw}^{sr}+\rho_{w}\phi_{bw}^{ref}+\rho_{o}\phi_{o}^{ref}\right)}+\frac{\rho_{w}\bar{\phi}_{vw}^{sr}}{\rho^{c}} \tag{12}$$

The above expressions were applied to obtain the mass density at 89 locations for which the mass fractions were found from the BSEM image. The resultant mass density maps of the three regions is shown in Fig. 7a, superimposed upon a C-scan SAM image of the tooth substrate. In the sound dentin (region 1), the mean mass density was found to be 1.79 ± 0.04 g cm^{-3}, which compares well with the specific gravity range of 1.64–2.09 reported for moist deciduous cavity-free dentin [40]. The mass density of the carious and the caries-affected dentin (regions 2 and 3) ranged from 1.21 to 2.03 g cm^{-3}, with a mean of 1.80 ± 0.22 g cm^{-3}. Alternatively, we can utilize Eqs. (8) and (9) directly, assuming that the caries and caries-affected regions develop prior to resorption. The difference in the calculated densities from the two methods is found to be less that 1%.

4.3. Microscale homotopic physico-mechanical properties

The homotopic measurements performed with SAM and BSEM allow us to obtain the micromechanical properties at a resolution of 120 μm. The reflection coefficients of the same three regions at the same locations and lateral resolution are shown in Fig. 7b (extracted from Fig. 5a). As a result, we can study the relationship between microscale elastic moduli, density and composition of sound, carious and caries-affected dentin for the primary tooth sample. In Fig. 7c, we show the corresponding acoustic impedance map superimposed upon a C-scan SAM image of the tooth substrate obtained from the reflection coefficients in Fig. 7b as follows:

$$Z=Z_{A}\frac{(1+R)}{(1-R)} \tag{13}$$

where Z is the acoustic impedance of the tooth substrate. This acoustic impedance was combined with the mass density, ρ, to obtain the constrained elastic modulus, denoted by C_{11} in Voigt notation, where 1 represents the direction normal to the tooth surface, using the following expression:

$$C_{11}=\frac{Z^{2}}{\rho} \tag{14}$$

The corresponding elastic moduli maps are plotted in Fig. 7d. Based upon the error estimates for the mean reflection coefficients, the error of the mean C_{11} is estimated to vary from 0.35% to 1.24% for dentin substrate reflection coefficients varying from 0.09 to 0.66. As expected, the elastic modulus varies significantly from location to location. In the sound dentin region, the mean elastic modulus was found to be 10 ± 2 GPa. These values are somewhat lower than the Young's moduli reported for inner primary tooth dentin at locations close to the pulp wall (ranging from 2.88 to 19.68 GPa in Angker et al. [38], and from 14.00 to 22.84 GPa in Hosoya and Marshall [36]). The low values observed in our measurement were likely caused by resorption prior to natural exfoliation. We further observe that in caries-affected locations (region 3 in Fig. 1) the elastic modulus is higher than the carious or sound dentin regions. Previous studies have indicated the presence of hypermineralized dentin or sclerotic dentin in the vicinity of carious lesions [61,62,64,65]. The higher values of elastic modulus could be

attributed to a higher level of mineralization in these locations. It is noteworthy, however, that sclerotic dentin is not always present below carious lesions [35]. The conditions under which hypermineralization occurs in proximity of carious dentin remains unclear and needs further investigation. In region 2, which comprises locations in carious dentin, the elastic modulus varies over a large range. It is well known that carious locations are highly heterogeneous, with widely varying degree and extent of demineralization.

Clearly, the mineral content has a significant effect on the elastic modulus. Previous investigators have attempted to correlate the mineral content to elastic modulus in dentin [2, 3]. Fig. 8 shows the plot of elastic modulus vs. the mass density and mineral volume fraction for the 89 locations displayed in Fig. 7. While, in general, the elastic modulus increases with mineral content and mass density, the correlation is quite weak. At a certain density and mineral volume fraction, the elastic modulus variation is found to be five times as large. Thus, the mineral content or density alone cannot be used to uniquely determine the elastic modulus. At the fundamental level, the interactions between collagen and nanocrystalline mineralite gives rise to the stiffness of the dentin structure. Indeed, the various efforts [67,68] to calculate calcified tissue moduli based upon constituent phases suggest that the mechanical behavior of these tissues at various hierarchical scales may not be determined by simply considering the composition but, rather, additional interaction at the collagen/mineral interface must be considered.

5. Conclusion

The main contribution of this paper is the development of a methodology for determining microscale elastic modulus and mass density of calcified tissue using homotopic measurements performed with SAM and BSEM. In particular, we have applied this methodology to characterize a second primary molar specimen exhibiting sound and caries-affected regions. The specimen was first imaged with SAM to obtain the microscale reflection coefficients, and subsequently acoustic impedance, at various locations on the sample. The advantage of using SAM is that the measurements are non-destructive and the sample is always in an aqueous environment, which is very important for biological materials. The sample is thus preserved in its near natural state for analysis with other non-destructive or destructive techniques. In this work, the same specimen was examined with BSEM and the backscattered images were analyzed to determine mineral mass fraction maps at the same lateral resolution as the SAM acoustic impedances. To ensure accuracy of our measurements, careful calibration was performed for both SAM and BSEM. The calibration process is especially important when highly heterogeneous substrates are imaged with SAM.

The specimen of primary tooth dentin analyzed in this paper exhibited the following unique characteristics. The specimen: (i) was likely undergoing resorption since it was collected upon normal exfoliation; (ii) had demineralized carious regions; and (iii) had hypermineralized caries-affected regions. To correctly account for resorption, demineralization and hypermineralization, relationships between measured mineral mass fraction and material mass density were derived for resorbing sound, carious and caries-affected dentin. These relationships were then used to determine the microscale mass density at the same lateral resolution and location as the SAM data. The data from SAM and SEM were combined to study the relationship between the elastic moduli and the micro-scale composition of sound to caries-affected dentin from a primary tooth. We found that, for the dentin sample used in this study, the correlation between elastic modulus and density or mineral content is very weak, and the elastic modulus cannot be uniquely determined by these parameters.

Acknowledgements

This research supported in part by: USPHS Research Grant NIH/NIDCR DE014392 (P.S.), National Institute of Dental and Craniofacial Research and USPHS Major Instrumentation Grant NIH/NIDCR S10 RR16710 (P.S.), USPHS Research Grant NIH/NIDCR K23 DE/HD00468 (B.B.) and NSF grant CMS-0506297 (A.M.). The authors gratefully acknowledge Dr.V. Dusevich for his help in performing the backscatter scanning electron microscopic analyses. The referees' comments contributed greatly to the final version of this paper, and for that we are very grateful.

References

1. Cowin, S. Bone mechanics. CRC Press; Boca Raton, FL: 2001.
2. Angker L, Nockolds C, Swain MV, Kilpatrick N. Correlating the mechanical properties to the mineral content of carious dentine – a comparative study using an ultra-micro indentation system (UMIS) and SEM–BSE signals. Arch Oral Biol 2004;49(5):369–78. [PubMed: 15041484]
3. Bembey, AK.; Oyen, ML.; Ko, C-C.; Bushby, AJ.; Boyde, A. Elastic modulus and mineral density of dentine and enamel in natural caries lesions. In: Fratzl, P.; Landis, WJ.; Wang, R.; Silver, FH., editors. Structure and mechanical behavior of biological materials. MRS; Warrendale, PA: 2005. p. 125-30.
4. Ferguson VL, Bushby AJ, Boyde A. Nanomechanical properties and mineral concentration in articular calcified cartilage and subchondral bone. J Anat 2003;203(2):191–202. [PubMed: 12924819]
5. Ferguson, VL.; Boyde, A.; Bushby, AJ. Elastic modulus of dental enamel: effect of enamel prism orientation and mineral content. In: Viney, C.; Katti, K.; Ulm, F-J.; Hellmich, C., editors. Mechanical properties of bioinspired and biological materials. MRS; Warrendale, PA: 2004. p. 3-8.
6. Tesch W, Eidelman N, Roschger P, Goldenberg F, Klaushofer K, Fratzl P. Graded microstructure and mechanical properties of human crown dentin. Calcif Tissue Int 2001;69(3):147–57. [PubMed: 11683529]
7. Gupta HS, Schratter S, Tesch W, Roschger P, Berzlanovich A, Schoeberl T, Klaushofer K, Fratzl P. Two different correlations between nanoindentation modulus and mineral content in the bone–cartilage interface. J Struct Biol 2005;149(2):138–48. [PubMed: 15681230]
8. Dickinson ME, Wolf KV, Mann AB. Nanomechanical and chemical characterization of incipient in vitro carious lesions in human dental enamel. Arch Oral Biol 2007;52(8):753–60. [PubMed: 17412307]
9. Katz JL, Meunier A. Scanning acoustic microscope studies of the elastic properties of osteons and osteon lamellae. J Biomech Eng 1993;115(4B):543–8. [PubMed: 8302038]
10. Turner CH, Rho J, Takano Y, Ting YT, Pharr GM. The elastic properties of trabecular and cortical bone tissues are similar: results from two microscopic measurement techniques. J Biomech 1999;32 (4):437–41. [PubMed: 10213035]
11. Raum K, Leguerney I, Chandelier F, Talmant M, Saïed A, Peyrin F, Laugier P. Site-matched assessment of structural and tissue properties of cortical bone using scanning acoustic microscopy and synchrotron radiation μCT. Phys Med Biol 2006;51(3):733–46. [PubMed: 16424592]
12. Raum K, Cleveland RO, Peyrin F, Laugier P. Derivation of elastic stiffness from site-matched mineral density and acoustic impedance maps. Phys Med Biol 2006;51(3):747–58. [PubMed: 16424593]
13. Hofmann T, Heyroth F, Meinhard H, Fränzel W, Raum K. Assessment of composition and anisotropic elastic properties of secondary osteon lamellae. J Biomech 2006;39(12):2282–94. [PubMed: 16144702]
14. Marshall GW, Marshall SJ, Kinney JH, Balooch M. The dentin substrate: structure and properties related to bonding. J Dent 1997;25(6):441–58. [PubMed: 9604576]
15. Gage, JP.; Francis, MJO.; Triffitt, JT. Collagen and dental matrices. Wright; Boston, MA: 1989. p. 1-24.
16. Linde A. Dentin matrix proteins: composition and possible functions in calcification. The Anatom Record 1989;224(2):154–66.
17. Butler WT. Dentin extracellular matrix and dentinogenesis. Oper Dent 1992;(Suppl 5):18–23. [PubMed: 1470547]
18. Arsenault AL. A comparative electron microscopic study of apatite crystals in collagen fibrils of rat bone, dentin and calcified turkey leg tendons. Bone Miner 1989;6(2):165–77. [PubMed: 2765707]

19. Wang R, Weiner S. Human root dentin: structure anisotropy and Vickers microhardness isotropy. Connect Tissue Res 1998;39(4):269–79. [PubMed: 11063007]
20. Manly RS, Deakins ML. Changes in the volume per cent of moisture, organic and inorganic material in dental caries. J Dent Res 1940;19(2):165–70.
21. Sumikawa DA, Marshall GW, Gee L, Marshall SJ. Microstructure of primary tooth dentin. Pediatr Dent 1999;21(7):439–44. [PubMed: 10633518]
22. Koutsi V, Noonan RG, Horner JA, Simpson MD, Matthews WG, Pashley DH. The effect of dentin depth on the permeability and ultrastructure of primary molars. Pediatr Dent 1994;16(1):29–35. [PubMed: 8015939]
23. Hirayama A, Yamada M, Miake K. An electron microscopic study on dentinal tubules of human deciduous teeth. Shikwa Gakuho 1986;86(6):1021–31. [PubMed: 3466350]
24. Weiner S, Veis A, Beniash E, Arad T, Dillon JW, Sabsay B, et al. Peritubular dentin formation: crystal organization and the macro-molecular constituents in human teeth. J Struct Biol 1999;126(1):27–41. [PubMed: 10329486]
25. Jones, SJ.; Boyde, A. Ultrastructure of dentine and dentinogenesis. In: Linde, A., editor. Dentine and dentinogenesis. Boca Raton, FL: CRC Press: 1984. p. 81-134.
26. Gruner JW, McConnell D, Armstrong WD. The relationship between crystal structure and chemical composition of enamel and dentin. J Biol Chem 1937;121(2):771–81.
27. Bird MJ, French EL, Woodside MR, Morrison MI, Hodge HC. Chemical analyses of deciduous enamel and dentin. J Dent Res 1940;19(4):413–23.
28. LeFevre ML, Hodge HC. Chemical analysis of tooth samples composed of enamel, dentine and cementum. II. J Dent Res 1937;16(4):279–87.
29. Kinney JH, Marshall SJ, Marshall GW. The mechanical properties of human dentin: a critical review and re-evaluation of the dental literature. Crit Rev Oral Biol Med 2003;14(1):13–29. [PubMed: 12764017]
30. Kinney JH, Balooch M, Marshall GW, Marshall SJ. A micromechanics model of the elastic properties of human dentine. Arch Oral Biol 1999;44(10):813–22. [PubMed: 10530914]
31. Katz JL, Bumrerraj S, Dreyfuss J, Wang Y, Spencer P. Micromechanics of the dentin/adhesive interface. J Biomed Mater Res B Appl Biomater 2001;58(4):366–71.
32. Lees S, Rollins FR. Anisotropy in hard dental tissues. J Biomech 1972;5(6):557–66. [PubMed: 4665892]
33. Kinney JH, Gladden JR, Marshall GW, Marshall SJ, So JH, Maynard JD. Resonant ultrasound spectroscopy measurements of the elastic constants in human dentin. J Biomech 2004;37(4):437–41. [PubMed: 14996555]
34. John C. Lateral distribution of ultrasound velocity in horizontal layers of human teeth. J Acoust Soc Am 2006;119(2):1214–26. [PubMed: 16521782]
35. Hosoya Y, Marshall GW. The nano-hardness and elastic modulus of carious and sound primary canine dentin. Oper Dent 2004;29(2):142–9. [PubMed: 15088724]
36. Hosoya Y, Marshall GW. The nano-hardness and elastic modulus of sound deciduous canine dentin and young premolar dentin-preliminary study. J Mater Sci Mater Med 2005;16(1):1–8. [PubMed: 15754137]
37. Hosoya Y, Tay FR. Hardness, elasticity, and ultrastructure of bonded sound and caries-affected primary tooth dentin. J Biomed Mater Res B Appl Biomater 2007;81B(1):135–41. [PubMed: 16941582]
38. Angker L, Swain MV, Kilpatrick N. Micro-mechanical characterisation of the properties of primary tooth dentine. J Dent 2003;31(4):261–7. [PubMed: 12735920]
39. Angker L, Nijhof N, Swain MV, Kilpatrick NM. Influence of hydration and mechanical characterization of carious primary dentine using an ultra-micro indentation system (UMIS). Eur J Oral Sci 2004;112(3):231–6. [PubMed: 15154920]
40. Boyd JD, Drain CL, Deakins ML. Method for determining the specific gravity of dentin and its application to permanent and deciduous teeth. J Dent Res 1938;17(6):465–9.
41. Manly RS, Hodge CH, Ange LE. Density and refractive index studies of dental hard tissues. II: Density distribution curves. J Dent Res 1939;18(3):203–11.

42. Berghash SR, Hodge HC. Density and refractive index studies of dental hard tissues. III: Density distribution of deciduous enamel and dentin. J Dent Res 1940;19(5):487–95.
43. Kinney JH, Marshall GW Jr, Marshall SJ. Three-dimensional mapping of mineral densities in carious dentin: theory and method. Scan Microsc 1994;8(2):197–205.
44. Briggs, GA. Acoustic microscopy. Clarendon Press; Oxford: 1992.
45. Raum K, Jenderka KV, Klemenz A, Brandt J. Multilayer analysis: quantitative scanning acoustic microscopy for tissue characterization at a microscopic scale. IEEE Trans Ultrason Ferroelect Freq Contr 2003;50(5):507–16.
46. Hirsekorn S, Pangraz S, Weides G, Arnold W. Measurement of elastic impedance with high spatial resolution using acoustic microscopy. Appl Phys Lett 1995;67(6):745–7.
47. Prasad M. Mapping impedance microstructures in rocks with acoustic microscopy. The Leading Edge 2001;20(2):172–9.
48. Katz JL, Spencer P, Nomura T, Wagh A, Wang Y. Micromechanical properties of demineralized dentin with and without adhesive infiltration. J Biomed Mater Res A 2003;66A(1):120–8. [PubMed: 12833438]
49. Marangos, O.; Katz, JL.; Wang, Y.; Spencer, P.; Misra, A. 2006 society of experimental mechanics annual conference and exposition. St. Louis, MO: 2006. Micromechanical property quantification using scanning acoustic microscopy. Paper #102
50. Taylor, JR. An introduction to error analysis. University Science Books; Sausalito, CA: 1997.
51. Banerjee A, Boyde A. Autofluorescence and mineral content of carious dentine: scanning optical and backscattered electron microscopic studies. Caries Res 1998;32(3):219–26. [PubMed: 9577988]
52. Roschger P, Fratzl P, Eschberger J, Klaushofer K. Validation of quantitative backscattered electron imaging for the measurement of mineral density distribution in human bone biopsies. Bone 1998;23 (4):319–26. [PubMed: 9763143]
53. Wieliczka DM, Spencer P, LeGeros RZ. Surface spectroscopy of apatitic materials: limitations and concerns. J Dent Res 1996;75(11):1865–70. [PubMed: 9003233]
54. LeGeros, RZ. Calcium phosphates in oral biology and medicine. Karger; Basel: 1991.
55. Hirayama A. Experimental analytical electron microscopic studies on the quantitative analysis of elemental concentrations in biological thin specimens and its application to dental science. Shikwa Gakuho 1990;90(8):1019–36. [PubMed: 2134979]
56. Handbook of chemistry and physics. Vol. 72nd ed.. CRC Press; Boston, MA: 1991.
57. Fels IG. Hydration and density of collagen and gelatin. J Appl Poly Sci 1964;8(4):1813–24.
58. Noda H. Partial specific volume of collagen. J Biochem 1972;71(4):699–703. [PubMed: 5042459]
59. Garberoglio R, Brännström M. Scanning electron microscopic investigation of human dentinal tubules. Arch Oral Biol 1976;21(6):355–62. [PubMed: 1066114]
60. Pashley DH. Dentin: a dynamic substrate – a review. Scan Microsc 1989;3(1):161–76.
61. Driessens, FCM.; Woltgens, JHM. Tooth development and caries. CRC Press; Boca Raton, FL: 1986. p. 132-137.
62. Nakajima M, Ogata M, Okuda M, Tagami J, Sano H, Pashley DH. Bonding to caries-affected dentin using self-etching primers. Am J Dent 1999;12(6):309–14. [PubMed: 10850253]
63. Zheng L, Hilton JF, Habelitz S, Marshall SJ, Marshall GW. Dentin caries activity status related to hardness and elasticity. Eur J Oral Sci 2003;111(3):243–52. [PubMed: 12786956]
64. Marshall GW, Habelitz S, Gallagher R, Balooch M, Balooch G, Marshall SJ. Nanomechanical properties of hydrated carious human dentin. J Dent Res 2001;80(8):1768–71. [PubMed: 11669491]
65. Ten Cate, AR. Repair and regeneration of dental tissue. In: Ten Cate, AR., editor. Oral histology. development, structure, and function. Mosby; St. Louis, MO: 1994. p. 456-68.
66. Arnold WH, Konopka S, Gaengler P. Qualitative and quantitative assessment of intratubular dentin formation in human natural carious lesions. Calcif Tissue Int 2001;69(5):268–73. [PubMed: 11768196]
67. Hellmich C, Ulm FJ, Dormieux L. Can the diverse elastic properties of trabecular and cortical bone be attributed to only a few tissue-independent phase properties and their interactions? Biomech Model Mechanobiol 2004;2(4):219–38. [PubMed: 15054639]

68. Nikolov S, Raabe D. Hierarchical modeling of the elastic properties of bone at submicron scales: the role of extrafibrillar mineralization. Biophys J 2008;94(11):4220–32. [PubMed: 18310256]

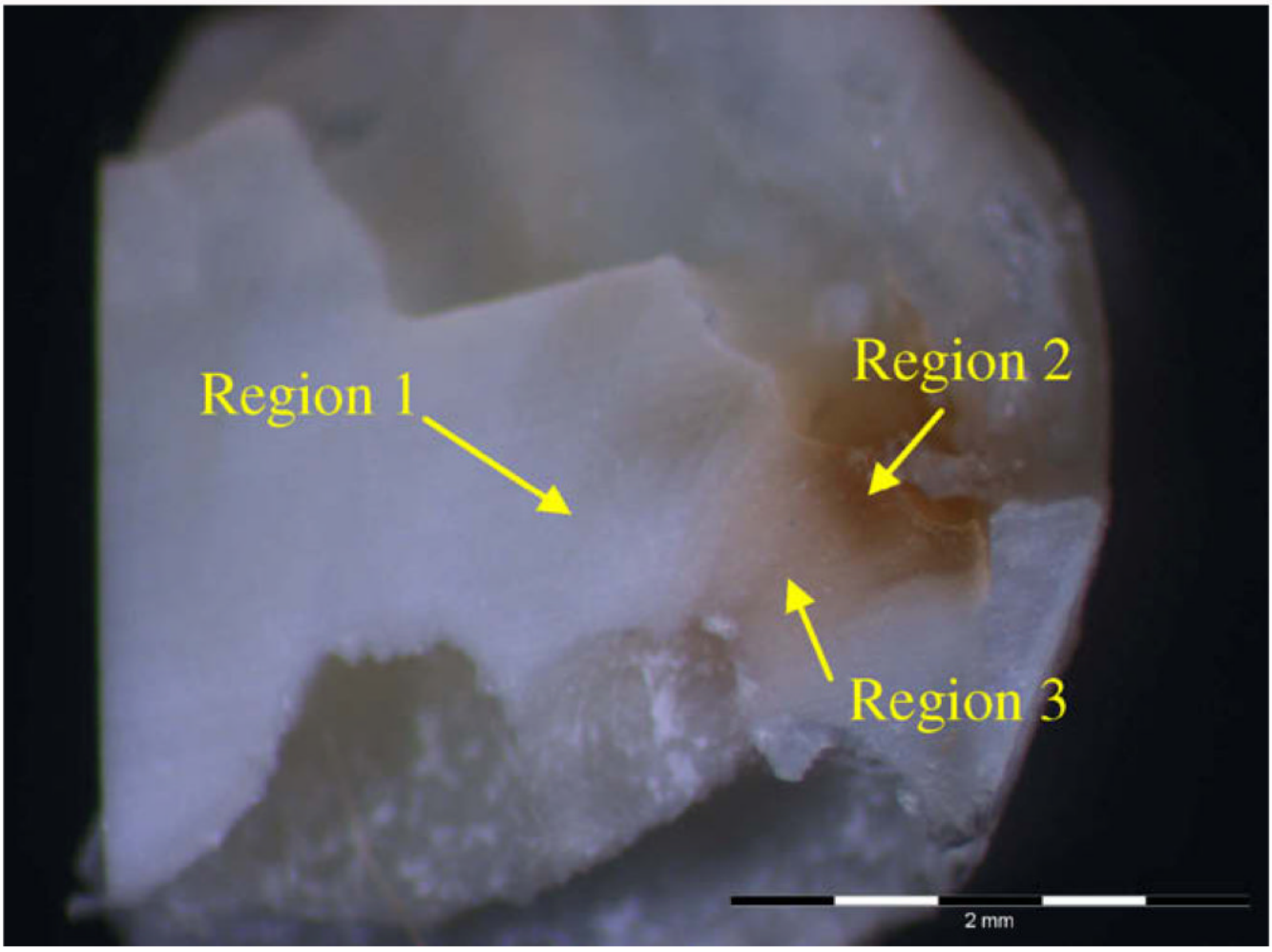

Fig. 1.
Optical image of the primary tooth section along the mesial–distal direction. Region 1 is considered to be sound dentin, region 2 is considered as carious dentin, while region 3 is identified as caries-affected dentin. Locations within regions 2 and 3 are intermingled with each other and cannot be easily demarcated.

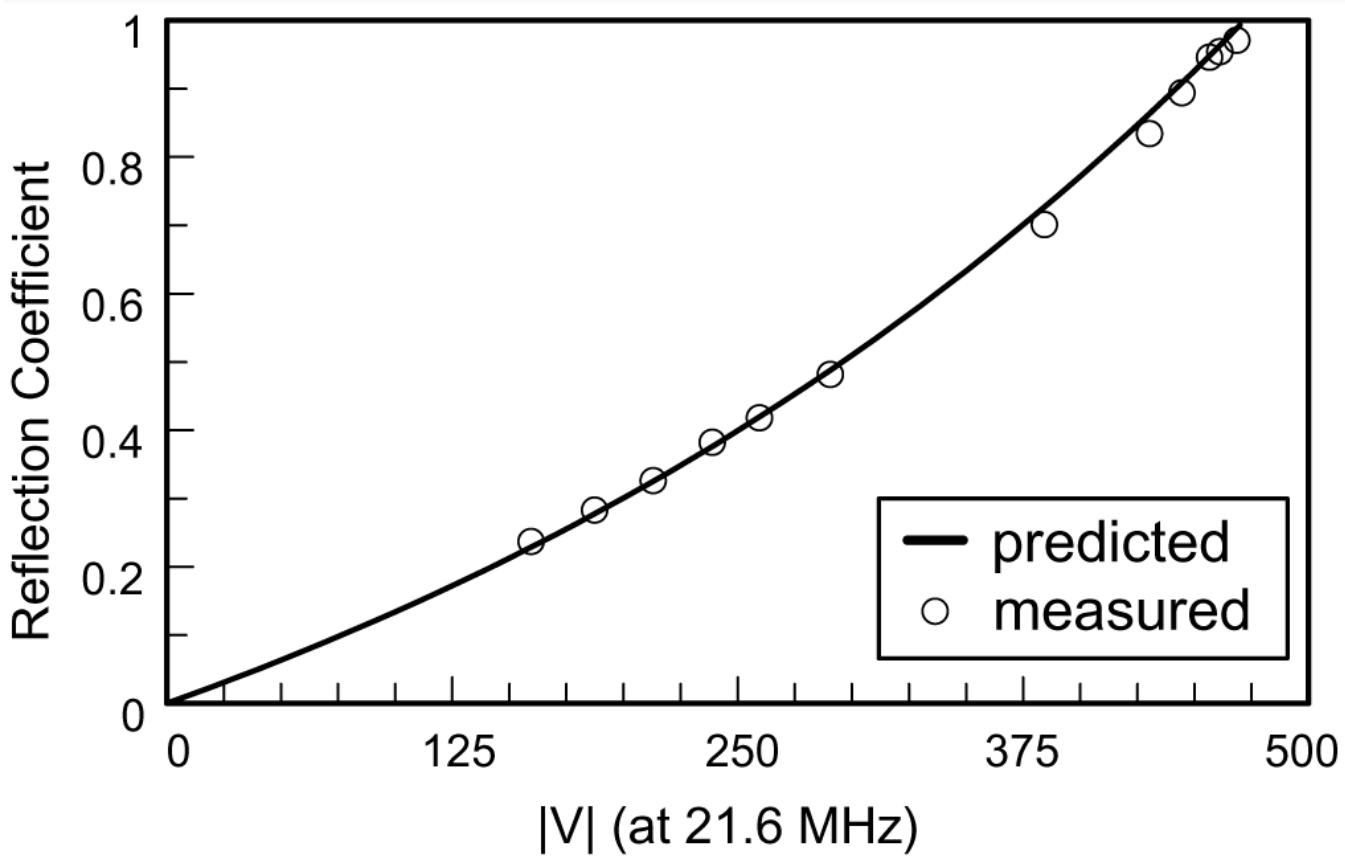

Fig. 2.
Predicted and measured relationship between Fourier amplitude and reflection coefficient for the 0 dB gain setting at the frequency of 21.6 MHz.

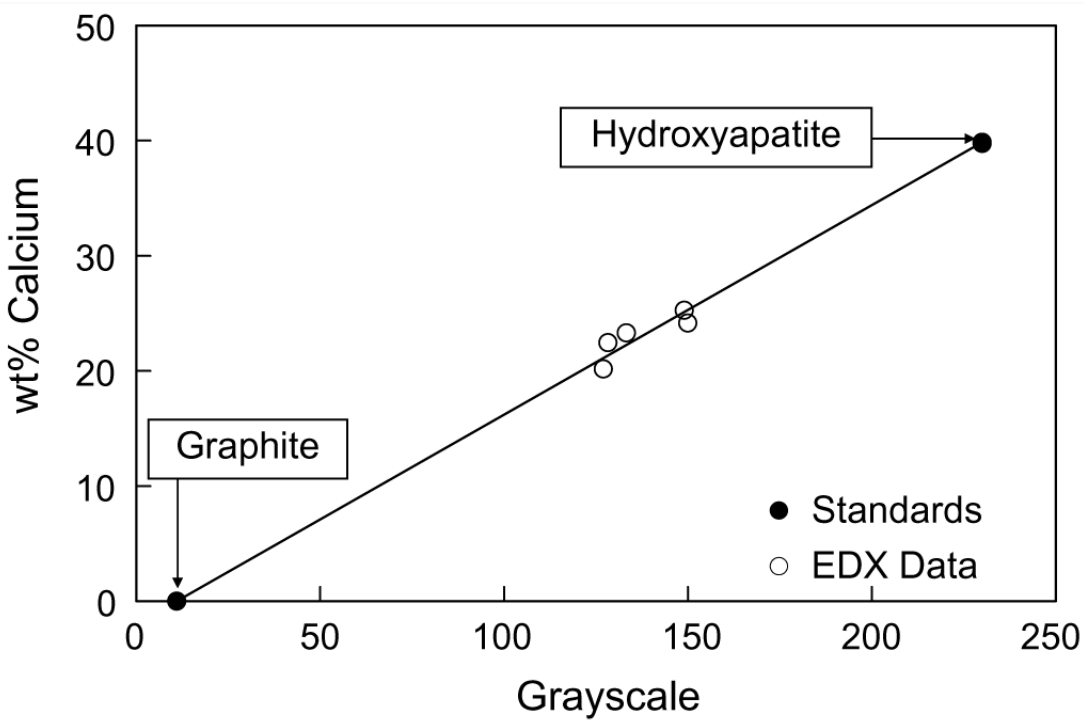

Fig. 3.
Calcium content vs. grayscale of the backscatter SEM micrographs obtained at ×50 magnification and 15.0 kV setting.

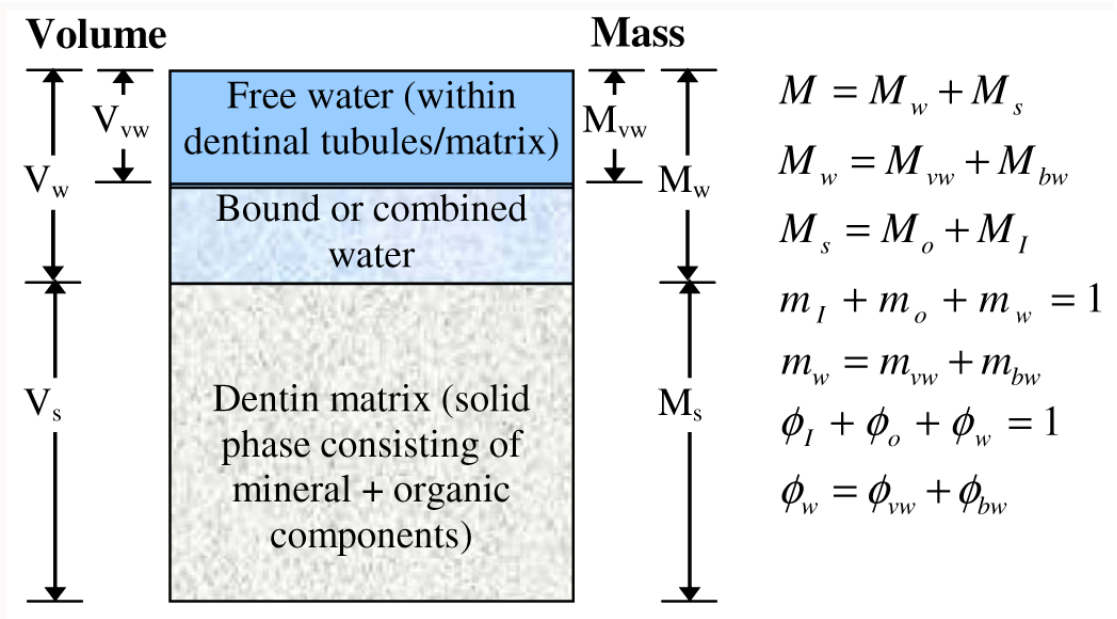

Fig. 4.
Schematic phase diagram of dentin composition and the mass and volume balance relationships.

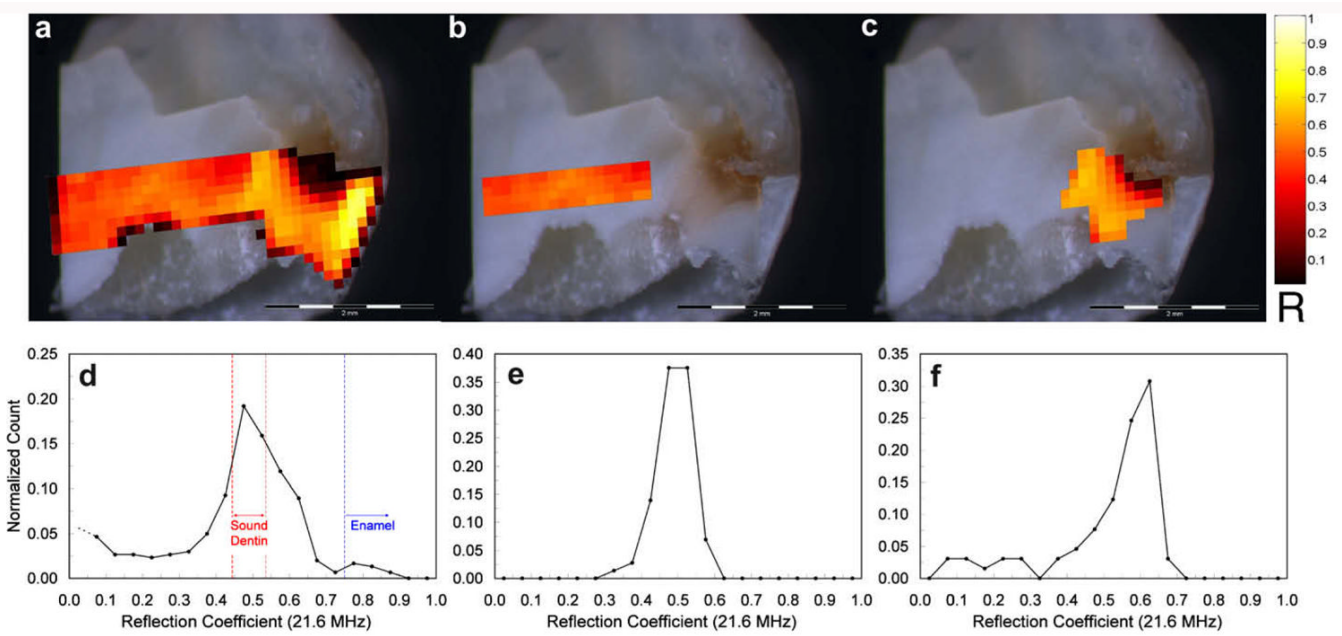

Fig. 5.

Optical image of the primary tooth section superimposed by SAM-measured reflection coefficients in hot colors: (a) all locations in regions 1–3; (b) locations in sound dentin – region 1; (c) locations in carious and caries-affected dentin – regions 2 and 3. (d)–(f) Histograms of reflection coefficients corresponding to (a)–(c).

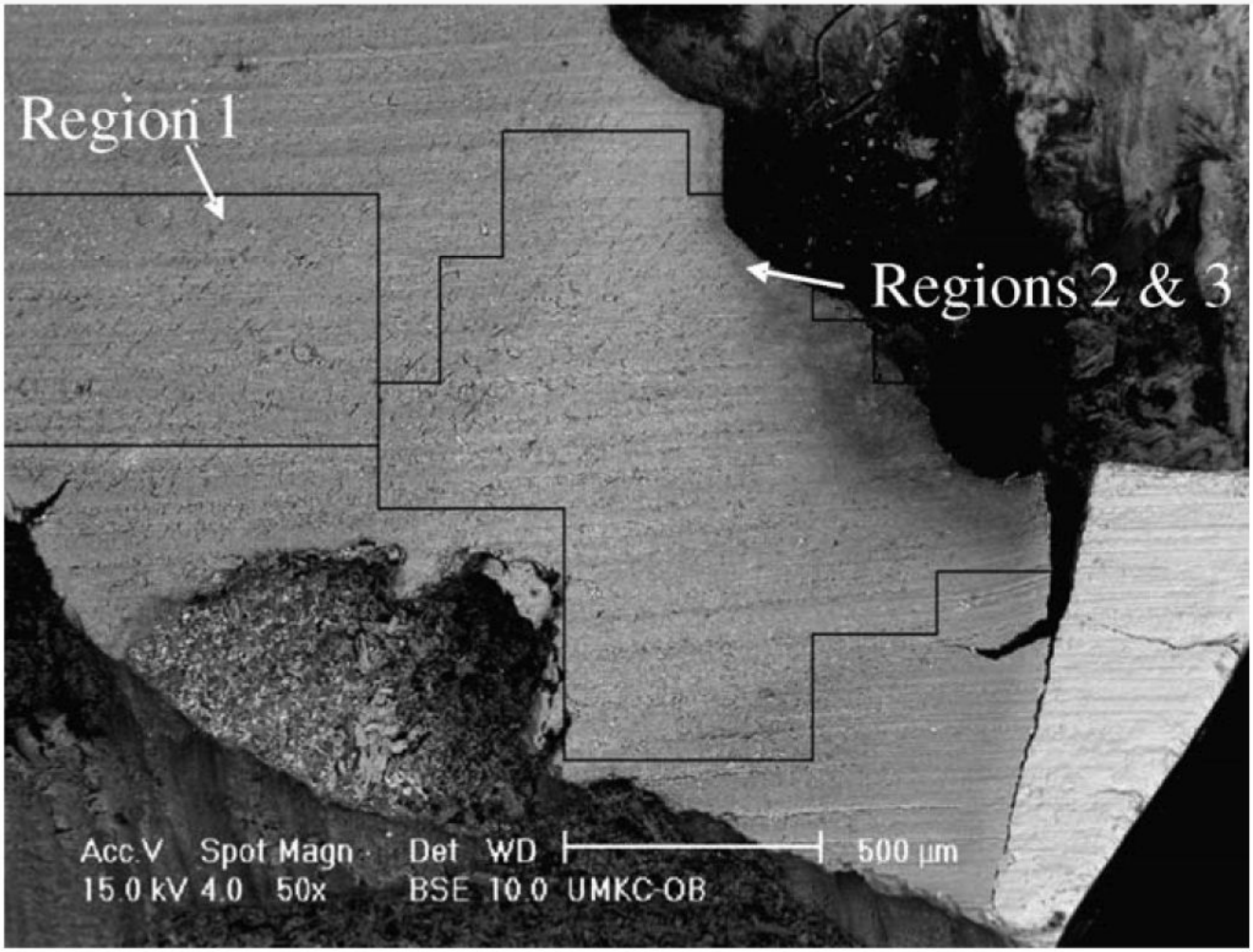

Fig. 6.
SEM backscatter image of the same primary tooth section used for SAM data collection. A subset of the tooth substrate corresponding to a portion of region 1 shown in Fig. 5b and regions 2 and 3 shown in Fig. 5c are used for analysis of the backscatter data.

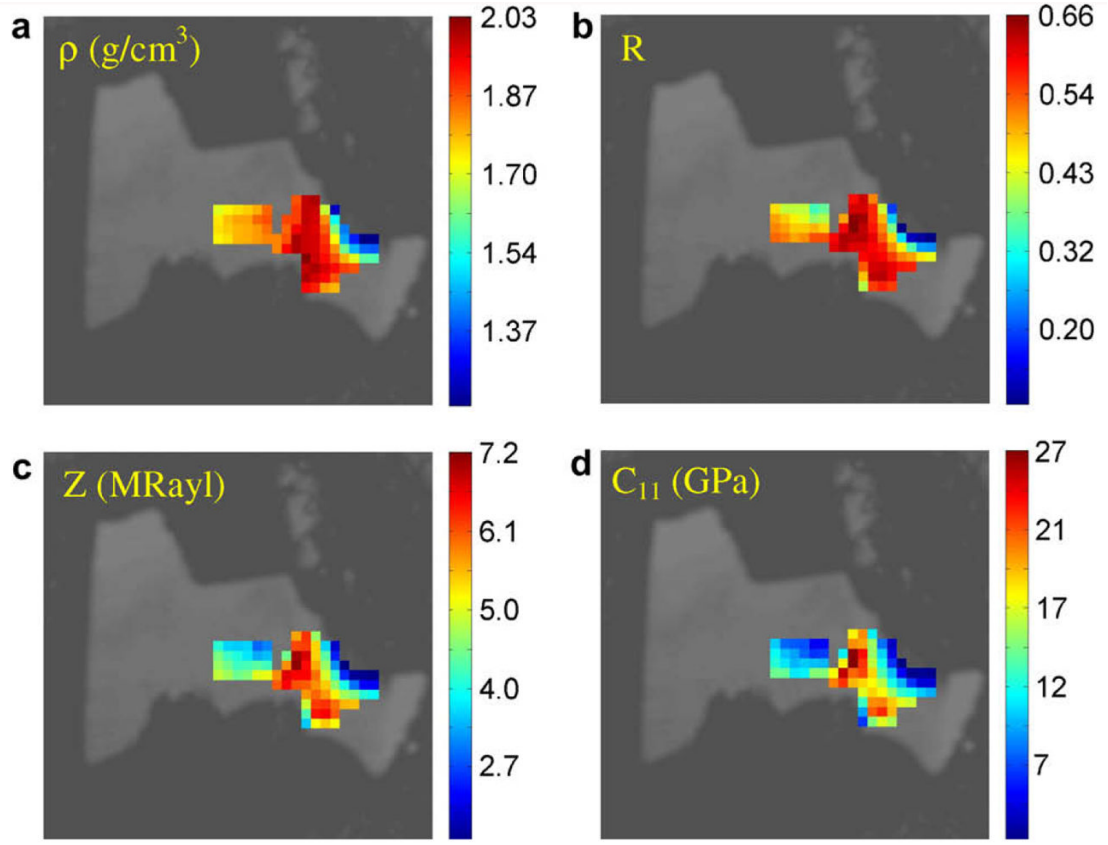

Fig. 7.
SAM image superimposed by (a) density, (b) reflection coefficient, (c) acoustic impedance and (d) elastic modulus.

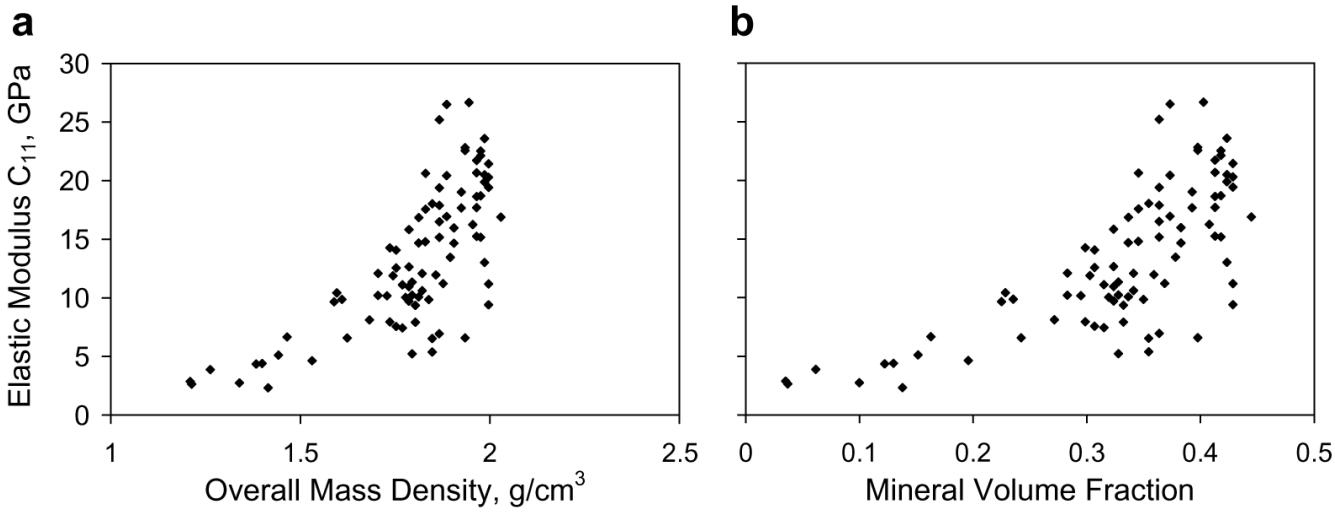

Fig. 8.
Elastic modulus plotted against (a) the mass density and (b) the mineral volume fraction (data from Fig. 7).

Table 1

Mass fraction, volume fraction and density of dentin components obtained from the literature.

Component	Density, ρ (g cm^{-3})	Sound permanent dentin		Sound primary tooth dentin	
		Mass fraction, m	Volume fraction, ϕ	Mass fraction, m	Volume fraction, ϕ
Mineral (I)	3.0	0.70	0.49	0.65	0.44
Organic (o)	1.4	0.20	0.30	0.25	0.36
Void water (vw)	1.0	0.08	0.17	0.08	0.16
Bound water (bw)	1.0	0.02	0.04	0.02	0.04